Journal of Geophysical Research: Earth Surface

Key Points:
- An increase in sediment cohesion promotes the development of deep and narrow channels and reduces lateral mobility
- The decrease in the mobility of sediment transport systems increases depositional persistence
- Cohesion aids the pumping of fine sand into deep marine and increases segregation between coarse sand and fine grains in the stratigraphy

Correspondence to:
Q. Li,
qli1@gatech.edu

Influence of Sediment Cohesion on Deltaic Morphodynamics and Stratigraphy Over Basin-Filling Time Scales

Qi Li[1,2] (iD), W. Matthew Benson[1], Margaret Harlan[1] (iD), Patrick Robichaux[3], Xiaoyu Sha[3], Kehui Xu[3,4], and Kyle M. Straub[1]

[1]Department of Earth and Environmental Sciences, Tulane University, New Orleans, LA, USA, [2]Department of Earth and Atmospheric Sciences, Georgia Institute of Technology, Atlanta, GA, USA, [3]Department of Oceanography and Coastal Sciences, Louisiana State University, Baton Rouge, LA, USA, [4]Coastal Studies Institute, Louisiana State University, Baton Rouge, LA, USA

Abstract Results from physical and numerical experiments suggest that sediment cohesion influences deltaic morphodynamics by promoting the development and maintenance of channels. As a result, cohesion is thought to increase the magnitude and time scales of internally generated (autogenic) processes and the dimensions of their stratigraphic products. We test these hypotheses by examining the surface processes and stratigraphic products from a suite of physical experiments where the influence of cohesion is isolated over temporal and spatial scales important for basin filling. Given the stochastic nature of autogenic sediment transport processes, we develop and employ a range of statistical tools and metrics. We observe that (1) an increase in sediment cohesion decreases lateral channel mobility and thus increases the time necessary to regrade deltaic surfaces; (2) enhanced channelization, due to sediment cohesion, increases the time necessary for the deposits of autogenic processes to average together and produce stratigraphic products with shapes set by the generation of regional accommodation; (3) cohesion promotes the transport of suspended sediment to terrestrial overbank and marine environments, which decreases the volume of channel, relative to overbank and marine deposits in the stratigraphic record. This increase in overbank and marine deposition changes the spatial distribution of sand in stratigraphy, with higher cohesion linked to enhanced segregation of fine particles from coarse sand in the experimental deposits. Combined, these results illustrate how the cohesion of sediment is fundamental in setting autogenic spatial and temporal scales and needs to be considered when inverting stratigraphic architecture for paleo-environmental history.

Plain Language Summary Sediment cohesion, which is mainly controlled by grain size and vegetation, promotes channelization on delta tops and increases the magnitude and time scales of internally generated processes, such as rapid changes of a river's couse. In this study, we use a suite of physical experiments to examine how sediment cohesion affects deltaic morphology and river dynamics and how these dynamics influence subsurface stratigraphy. We documented that an increase in sediment cohesion reduces lateral mobility of river channels and increases depositional persistence. In addition, cohesion promotes the pumping of fine materials to the terrestrial overbank and deep marine and thus increases the segregation between coarse sand and fine materials in the resulting stratigraphy. These findings can advance our ability to link surface dynamics with subsurface architecture and extract paleo-environmental signals from stratigraphy.

1. Introduction

Deltaic morphology is set by a plethora of forcings originating from both terrestrial and marine environments. Of these, the most frequently discussed are the flux of sediment to the shoreline and the wave and tide climates summarized in Galloway's (1975) ternary diagram. However, over the last decade more attention has been placed on the properties of sediment delivered to the coast. During this time, field (Burpee et al., 2015; Davies & Gibling, 2010; Gibling, 2006), numerical (Caldwell & Edmonds, 2014; Edmonds & Slingerland, 2010), and laboratory (Hoyal & Sheets, 2009; Martin et al., 2009; Peakall, Ashworth, & Best, 2007; Straub, Li, & Benson, 2015; Tal & Paola, 2010) studies highlighted the importance of sediment cohesion to the morphology and stratigraphy of rivers and deltas. These studies emphasize that sediment cohesion is as important as the volumetric sediment flux, wave and/or tide climate to the evolution of river deltas over lobe-building time scales. However, few studies have explored the implications of sediment cohesion on

surface processes and stratigraphy over the spatial and temporal scales important for filling alluvial basins. The primary aim of this study is to fill this knowledge gap.

While studies conducted over the last decade expanded our appreciation of the implications of cohesive sediment to deltaic morphodynamics, sediment properties, including cohesion, have long been discussed. For example, Kolb (1963) noted an increase in Pleistocene clays in the downstream direction in a study of the Mississippi River Delta. He hypothesized that these cohesive sediments promoted the development of narrow and deep channels with slow migration rates. Studies by Orton and Reading (1993) and Tornqvist (1993) also indicated the influence of fine-grained and cohesive sediments on channel migration rates and the geometry of deltaic channels in both cross section and planform.

Many factors influence sediment cohesion, including the grain size, mineralogy, and compaction history of sediment, and the density and type of riparian vegetation (Davies & Gibling, 2011; Grabowski, Droppo, & Wharton, 2011). Focusing first on sediment grain size, a suite of recent numerical experiments explored the influence of cohesion on deltaic morphodynamics by employing algorithms that link the critical shear stress for initiation of sediment motion, τ_{cr}, to sediment properties, including cohesion (Burpee et al., 2015; Caldwell & Edmonds, 2014; Edmonds & Slingerland, 2010). In many of these models particles finer than silt are assumed to be somewhat cohesive, so the finer the median particle size of the bed, the more cohesion is assumed. These studies suggest that decreasing grain size (with associated increases in sediment cohesion) fundamentally changes the shape and depositional patterns of river deltas over lobe-building time scales. For example, Edmonds and Slingerland (2010) and Caldwell and Edmonds (2014) observe that deltas built from highly cohesive sediment form "bird's-foot" morphologies with rugose shorelines, whereas systems characterized by less cohesive sediment result in fan-like deltas with smooth shorelines.

Vegetation can also impart a strong control on the morphodynamics of deltas, partially due to its influence on sediment cohesion (Hicks et al., 2002; Murray & Paola, 2003; Nardin & Edmonds, 2014; Rosen & Xu, 2013). For instance, Murray and Paola (2003) use a cellular model to explore the influence of roots on channel patterns. This model suggests that roots aid river bank stabilization which can convert an otherwise braided system to a single thread channel, which has also been observed in physical experiments (Braudrick et al., 2009; Tal & Paola, 2007). The influence of vegetation on paleo-channel morphodynamics can also be inferred from stratigraphy. Davies and Gibling (2010, 2011) documented the evolution of channel patterns through geological time in response to the evolution of land plants. They showed that stratigraphy of channelized sections dated to pre-Devonian times, and thus prior to vascular land plants, have few single thread channel-bodies.

While the work highlighted above demonstrates the importance of sediment cohesion, we still lack a clear picture as to how this influences deltaic stratigraphy over the spatial and temporal scales important for alluvial basin filling. For example, how do cohesive channel deposits stack together and how do they differ from the stacking of noncohesive deposits? Does the introduction of cohesive sediment fundamentally change the partitioning of sediment between channels and their overbanks, and if so, how might this influence the segregation of fine from coarse sediment in their deposits? These questions are intertwined with the spatial and temporal scales of internal (autogenic) processes in deltaic morphodynamics including river avulsion, lobe switching, and other processes that result in sediment storage and release (Beerbower, 1964; Paola, 2016).

Straub et al. (2015) took a few initial steps in the exploration of the influence of cohesion on morphodynamics and stratigraphic architecture over basin-filling time scales. They conducted a set of physical experiments where the influence of sediment cohesion was isolated. In each experiment a self-organized delta was constructed through the introduction of water and sediment into an experimental basin that had a constant background base level rise, which promoted the development of tens of channel-depth worth of stratigraphy. The constant forcing in each experiment allowed autogenic spatial and temporal scales to be isolated and explored. Their study focused on the influence of cohesion in setting autogenic shoreline dynamics and on deltaic sediment retention rates. They found that enhanced channelization resulting from sediment cohesion reduces sediment retention rates and increases the autogenic temporal and spatial scales of shoreline transgressions and regressions.

In this study, we use the same set of physical experiments as Straub et al. (2015) but further the scope of exploration. Here the focus is on the stratigraphic implications of changes to deltaic morphodynamics induced by sediment cohesion. Given the stochastic nature of many autogenic surface processes and their

stratigraphic products (Paola, 2016), we take a statistical approach. This includes the use of previously developed metrics and the development of new metrics to quantify the temporal and spatial scales of autogenic processes and the partitioning of sediment by grain size in the final deposit. We start by confirming in our experiments that an increase in sediment cohesion promotes the development of deep and narrow channels that are less laterally mobile. We then test two main hypotheses that relate surface processes to stratigraphic products. First, we hypothesize that decreases in the mobility of river channels translate into increased persistence of depositional trends. This increased persistence is hypothesized to result from the deposition in and close to laterally stable channels. Second, we hypothesize that the development of deeper channels with lower migration rates enhances the segregation of fine from coarse sediments in the resulting stratigraphy by reducing the reworking of overbank deposits by channels and promoting the transport of fine sediments to overbank settings.
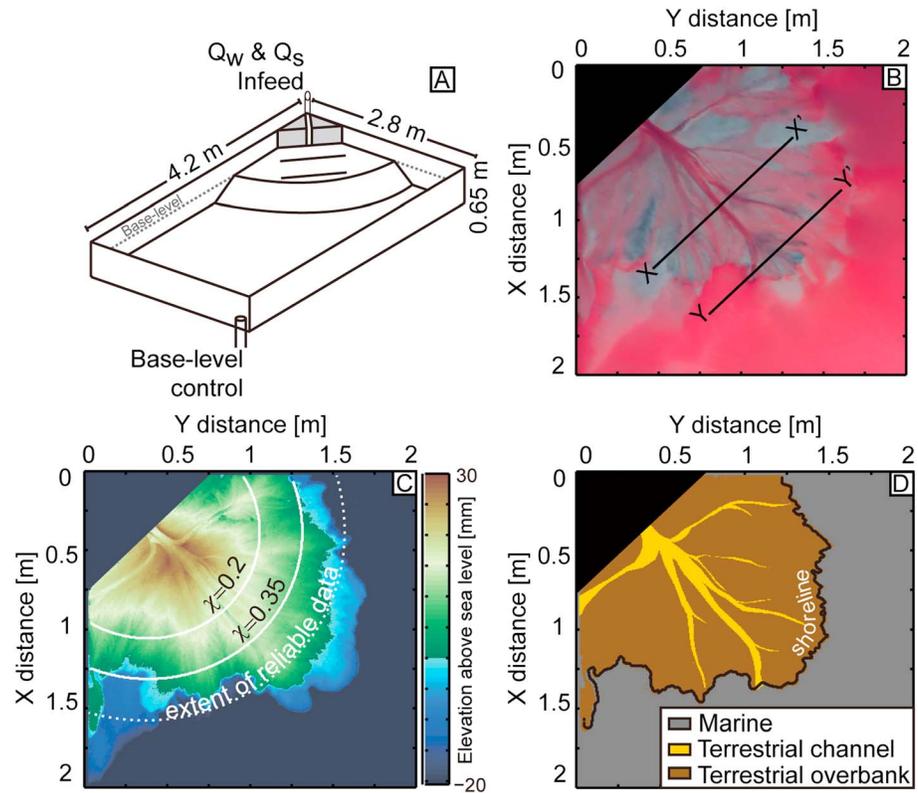
2. Methods

2.1. Physical Experiments

To examine the influence of sediment cohesion on deltaic surface dynamics and the resulting stratigraphy over spatial and temporal scales important to alluvial basin filling, we analyze data from three stages of two experiments (Figure 1).

The three experimental stages were conducted in the Tulane University Delta Basin, which is 2.80 m wide, 4.20 m long, and 0.65 m deep (Figure 1). These stages shared identical forcing conditions with the exception of the cohesion of sediment entering the basin. Accommodation was created at a constant rate in all experiments by increasing ocean level utilizing a motorized weir that is in hydraulic communication with the basin. Raising ocean level is similar to the generation of accommodation through subsidence in field-scale systems. The computer controlled ocean level rise rate ($r = 0.25$ mm/h) and input water ($Q_w = 1.72 \times 10^{-4}$ m^3/s) and sediment discharge ($Q_s = 3.91 \times 10^{-4}$ kg/s) were constant in all experiments. As such, shorelines were approximately at a constant location from the basin entrance, but with superimposed fluctuations associated with autogenic processes. The input sediment mixture was designed to mimic earlier experimental work conducted by ExxonMobil (Hoyal & Sheets, 2009) and had a broad particle size distribution, ranging from 1 to 1000 μm with a mean of 67 μm and was dominantly quartz that was white in color. One quarter of the coarsest 23.5% of the distribution was commercially dyed to aid visualization of stratigraphic architecture. The only difference in forcing conditions between the three experimental stages was the amount of the added polymer in the input sediment. This polymer (New Drill Plus distributed by Baker Hughes Inc.) enhances cohesion, which acts as a general proxy for the effect of consolidation, vegetation, and/or dewatered clays and enables the formation of deltas with strong channelization at subcritical Froude numbers. As discussed by Hoyal and Sheets (2009), a volumetrically small amount of this polymer in dry granular form, when combined with water, coats a fraction of the sediment grains with a viscous and cohesive film.

The three stages were performed over the course of two experiments. These two experiments were first discussed in Straub et al. (2015). Here we expand on their interpretation, with an enhanced focus on the resulting stratigraphy. The first experiment began with the progradation of a delta into a constant ocean level for 75 h, followed by 300 h of aggradation promoted by base level rise. Input sediment during this stage contained no polymer and as such was only weakly cohesive due to particle electrostatic forces. We refer to this as the weakly cohesive stage. A second stage was run for 700 h directly on top of the first stage. This stage included 40 g of dry granular polymer per 54 kg of sediment and had the same base level rise rate as the weakly cohesive stage. We refer to this as the moderately cohesive stage. The change in sediment cohesion at the start of the second stage resulted in the incision of channels into the weakly cohesive deposit. To isolate the characteristics of the moderately cohesive stage, we focus our analysis on the final 500 h of this stage. A strongly cohesive stage was conducted as part of a second experiment. This experiment also began with the progradation of a delta into an ocean of fixed depth, followed by aggradation driven by base level rise. Unfortunately, input Q_s during this initial aggradation was below our target rate. Following a brief pause in base level rise and adjustment of Q_s, we ran the main phase of this experiment for 900 h. This stage shares the same Q_w, Q_s, and ocean level rise rate as the first experiment but contains 80 g of polymer added per 54 kg of sediment. As such we refer to this as the strongly cohesive stage. While slight differences in initial ocean level and initial delta size exist between stages, the run time in each stage was long enough to

Figure 1. Schematic of experimental setup and maps illustrating types of data collected over the course of each experimental stage. (a) Schematic diagram of Tulane Delta Basin with key basin dimensions and controls labeled. (b) Characteristic digital image of the moderately cohesive experiment with flow on and dyed for visualization. Image collected with laser scanner such that all pixels are referenced relative to the basin coordinate system. Locations of physical stratigraphic sections are shown by solid black lines. (c) Digital elevation model (DEM) of experimental surface collected with laser scanner. Locations of synthetic stratigraphic sections from Figure 7 are shown by solid white lines. The dashed white line shows the extent of DEMs where topography was reliably measured for each run hour. (d) Map of depositional environment. Channel locations were manually mapped from digital images and coupled to topography and sea level history to define three environments. The solid black line denotes shoreline.

generate tens of channel-depth worth of stratigraphy, which we assume minimizes the effect of initial conditions on the bulk trends discussed below.

Topography was monitored with a 3-D laser scanner, resulting in digital elevation models (DEMs) with a 5 mm horizontal grid in the along- and across-basin directions and a vertical resolution <1 mm for terrestrial regions and areas with water depths <50 mm. In regions with water depths greater than 50 mm the laser scanner either did not return measurements or returned measurements with a high degree of noise, as assessed in calibration tests. One scan was taken near the end of each run hour with the flow on and dyed for visualization. These DEMs are coregistered with digital images collected by the scanner which allows the flow field to be directly tied to topography. A second scan was collected at the end of each run hour with the flow off for the highest possible resolution. Due to data gaps in regions of deep water in distal basin locations, we limit our analysis to a region defined by a radius of 1.3 m from the basin entrance. This region was generally either delta top or upper delta foreset over the course of each experiment. This spatial and temporal resolution was sufficient to capture the mesoscale morphodynamics of the delta-top systems (e.g., channel and lobe avulsions). We also collected digital images of the active delta top with a Cannon G10 camera every 15 min with input water dyed to further aid morphodynamic analysis.

Finally, at the end of each experiment, we sectioned the deltaic deposits along cross-sectional transects at 0.89 m and 1.30 m from the basin infeed point (Figure 1b). This was done by inserting a metal wedge into the deposit after the water level in the basin was raised to an elevation that flooded the entire deposit. The metal wedge was then filled with dry ice and methanol, which resulted in a chemical reaction that

lowered the temperature of the wedge to a value sufficient to freeze the pore water and the surrounding deposit to the wedge. The wedge was then extracted from the basin, providing a view of the preserved stratigraphy that was then photographed with digital cameras. While not quantified, we assume that minimal deformation of the deposit occurred during sampling. This assumption in based off similar depositional geometries observed in the synthetic and physical stratigraphy.

2.2. Gust Erosion Microcosm System Erodibility Experiments:

Several recent studies have used New Drill Plus to enhance sediment cohesion in deltaic experiments (Hoyal & Sheets, 2009; Martin et al., 2009; Straub et al., 2015). However, only Kleinhans et al. (2014) attempted to quantify how the polymer influences the shear stress necessary for initiation of sediment motion following sediment deposition. They used a direct shear test to measure the strength of a cohesive sediment mixture. For this type of test, the sample needs to be fully saturated and in well-drained conditions. However, the cohesiveness and low permeability of the sediment mixture prevent the cohesive sediment mixture from draining well. As a result, Kleinhans et al. found it unsuitable to quantify the cohesion of a sediment mixture similar to ours from a direct shear test. We attempted to quantify this cohesion using a dual-core Gust Erosion Microcosm System (GEMS) (Gust & Müller, 1997). To do this, we conducted an additional experiment with the same forcing conditions as the previously discussed experiments. This experiment included four stages: (1) 60 h of progradation, (2) 80 h of aggradation with a feed of weakly-cohesive sediment, (3) 80 h of aggradation with a feed of moderately-cohesive sediment, and (4) 80 h of aggradation with a feed of strongly-cohesive sediment. At the end of each stage, two cores were collected, at least 6.5 cm long, from the deltaic deposits using two 10 cm outer diameter push corers.
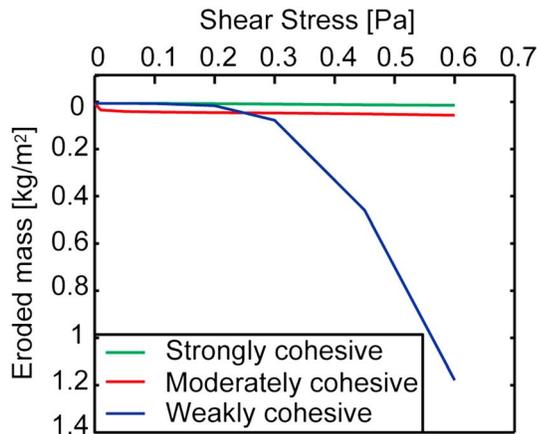
Immediately following collection of the cores, we measured the erodibility of the sediment cores by applying seven successive shear stresses (0.01, 0.05, 0.10, 0.20, 0.30, 0.45, and 0.60 Pa) to each core. Each stress level was maintained steady for about 20 min. When the applied shear stress is greater than the critical shear stress of the sediment, the sediment surface of the core starts to erode. The eroded materials were suspended and passed through a turbidimeter and collected in bottles. Through filtration of collected turbidity solutions, we measured the eroded mass for each imposed shear stress, which is used to generate eroded mass curves for each experimental sediment mixture. More methodological details can be found in Xu et al. (2016).

3. Results

In this section, we first present results from the GEMS experiment to characterize the influence of the polymer on sediment cohesion. Next, we characterize statistically how sediment cohesion influences the morphology and dynamics of the depositional system. Our aim is to characterize the full temporal and spatial scales important for autogenic surface dynamics and further quantify how sediment cohesion reduces morphodynamic rates (e.g., Edmonds & Slingerland, 2010; Hoyal & Sheets, 2009). Next, we characterize the stratigraphic architecture of each experimental stage. This includes statistical characterizations of stacking patterns, the spatial distribution of fine and coarse sediment in the deposit, and the volumes of sediment deposited in key depositional environments (terrestrial channel, terrestrial overbank, and marine). Here the goal is to test our hypothesis that changes in morphodynamics induced by cohesion are linked to specific stratigraphic consequences. We test our hypotheses with a suite of statistical metrics that are presented below. For each metric we start by highlighting the surface process or stratigraphic attribute which is being characterized and how this metric will test our central hypotheses. We then present theory which underpins each metric and the methods used to implement the measurements. This is immediately followed by the results of each analysis for our three experimental stages.

3.1. Erodibility Measurement

Several studies note the difficulty in accurately predicting and measuring the erodibility of cohesive sediment (Grabowski et al., 2011; Kleinhans et al., 2014). In this study, we attempt to overcome this through the use of a dual-core GEMS. Specifically, we measured eroded mass under each applied shear stress level for each experimental stage (Figure 2). In the weakly cohesive stage, the eroded mass increases as the applied shear stress increases. However, the eroded mass curve is almost flat and near zero for the moderately and strongly cohesive stages. These results indicate a significant difference in the erodibility between the weakly and the moderately/strongly cohesive sediment mixture. Our results likely indicate that the maximum shear stress level at 0.6 Pa generated by the GEMS system is less than the critical shear stresses for
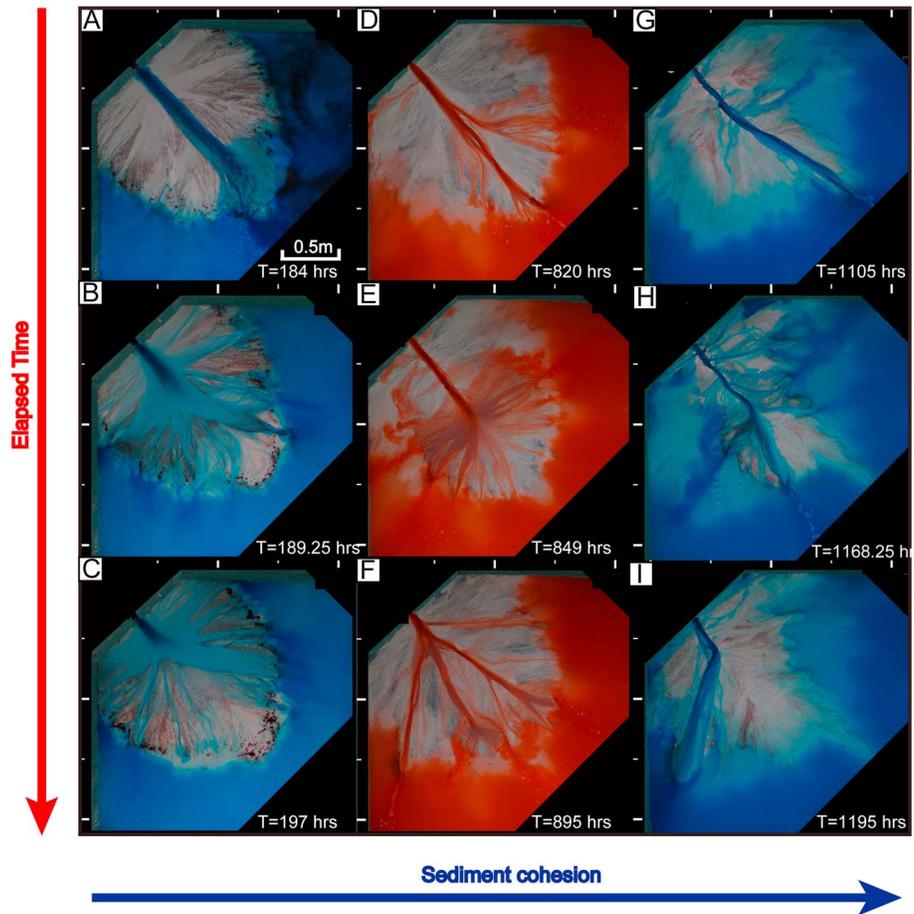
Figure 2. Measurements of eroded mass due to increasing applied shear stress to cores of experimental deposits in GEMS experiments. Two sediment cores in each experiment produce two eroded mass curves. Here we average two eroded mass curves to determine the final eroded mass curve in each experiment shown in this figure to compare difference in erodibility among sediment mixtures.
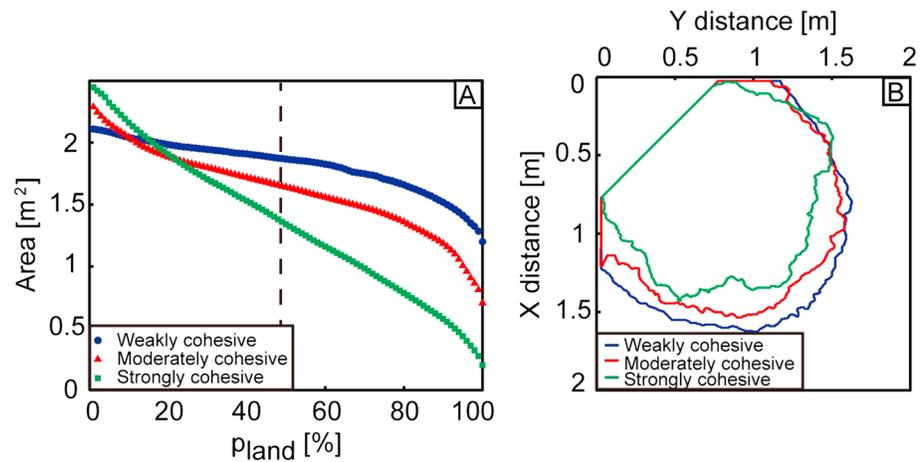
moderately/strongly cohesive sediment suspension. However, our results in Figure 2 clearly suggest that the presence of polymer in the sediment mixture increases the critical shear stress of the sediment. Given the difficulty in measuring this cohesion and other inherent scaling difficulties, we make no formal attempt to upscale our experiments to field scale but rather treat them as small systems of and to themselves (Hooke, 1968).

3.2. Flow Patterns

We start our analysis by noting several qualitative differences in the flow patterns of the three stages. In the weakly cohesive stage rapid lateral spreading of the flow at the entrance to the basin resulted in shallow flow thicknesses. This forced sediment to be transported within several grain diameters of the bed. Similar to previous studies (e.g., Kim & Jerolmack, 2008) that utilized weakly cohesive sediment, we observed a morphodynamic cycle characterized by sheet flow deposition which steepened the transport slope followed by the development of an erosional channel. This erosional channel lowered the transport slope and induced channel backfilling, initiating a new cycle of sheet flow and transport slope steepening (Figures 3a–3c).

Figure 3. Overhead images of the three experiments. Each experiment experienced repeated cycles of autogenic channel formation, back stepping, and avulsion. As cohesion increased this process occurred over longer time scales, channel lateral mobility decreased, and shoreline variability increased. (a–c) The weakly cohesive experiment. (d–f) The moderately cohesive experiment. (g–i) The strongly cohesive experiment.

Figure 4. Data defining (a) the experimental area that was above sea level for different percentages of run-time in the three experimental stages and (b) the shape of the delta area that was above sea level for at least 50% of each experimental stage.

The moderately and strongly cohesive experiments were also dominated by a morphodynamic channel cycle. However, this cycle was characterized by the following sequence. Preferential flow paths developed from unconfined flow following channel avulsions. These flow paths developed into channels through a mixture of erosion and aggradation of levees. Channels then prograded into the basin until a reduced channel slope and deposition of a mouth bar induced a morphodynamic backwater effect (Hoyal & Sheets, 2009). This resulted in channel backfilling until the flow found a weak spot in the channel bank, at which point an avulsion occurred and a new cycle began (Figures 3d–3i).
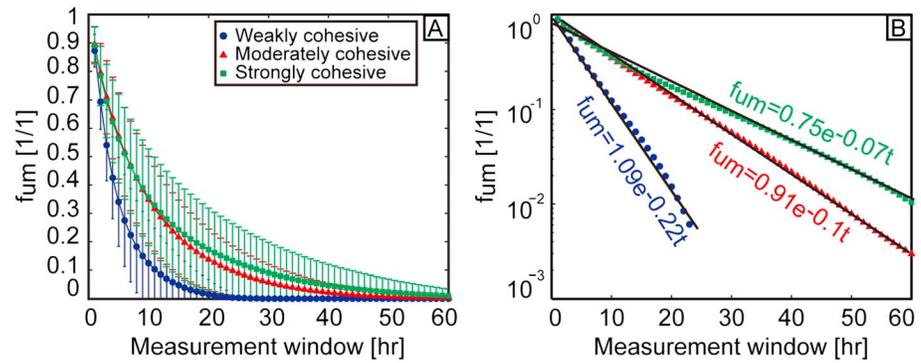
3.3. Delta-Top Area

To test how sediment cohesion affects the partitioning of sediment between terrestrial and marine settings, we quantify how the area of each delta changed as a function of the percent of time that area was above sea level, p_{land}. Specifically, we use the topographic maps and our time series of imposed sea level to extract all delta-top pixels above sea level for each run hour. Next, we calculate the percentage of time that each delta-top cell was above sea level. Each terrestrial delta cell is converted to an area equal to 2.5×10^{-5} m^2, determined by the geometry of the imposed topographic grid. Finally, we calculate how the area of the delta changed as a function of the minimum percent of time that area was above sea level.

In our experiments, periods of stable channelization result in large autogenic transgression, as deposition was focused at channel tips in relatively deep water (Figures 3d and 3g) (Straub et al., 2015). As a result, portions of the delta top transition between marine and terrestrial environments. On the three curves in Figure 4a, the value of delta-top area at $p_{land} = 100\%$ represents the surface area that is above sea level in all DEMs. We note that the area of the delta that is always above sea level is greatest for the weakly cohesive stage at approximately 1.2 m^2. In comparison, the area that is always above sea level for the moderately and strongly cohesive stages is 0.71 m^2 and 0.2 m^2, respectively. As p_{land} decreases, the area increases, and the rate of this increase is proportional to the cohesiveness of the sediment. As a result, the strongly cohesive stage actually has the largest area that was above sea level in at least one DEM, $p_{land} = 1\%$.

3.4. Time Scales of Surface Modification

Similar to previous studies that use overhead images to calculate time scales of channel mobility (Cazanacli, Paola, & Parker, 2002; Kim, Sheets, & Paola, 2010; Straub & Wang, 2013; Wickert et al., 2013), we are interested in characterizing the mobility of the transport systems in our experiments. These earlier studies detail how autogenic mobility is critical for determining the lateral distribution of sediment in basins, time gaps in the stratigraphic record, and the response to tectonic forcings. First, we characterize the total mobility of the transport system by tracking the fraction of the delta that has experienced geomorphic change (either erosion or deposition) regardless of what environment that change occurred in. Next, we characterize the mobility of the

Figure 5. Data defining the reduction in area that has not experienced topographic modification. (a) Data in arithmetic space, with mean decay trend represented by symbols. The vertical bars represent variability in measurements and are equal to ±1 standard deviation. (b) Decay of mean trend in semilog space to illustrate approximate exponential reduction in f_{um}, which is the fraction of delta-top area that has not been modified by a depositional or erosional event of at least 1 mm. Equations of best fit trends lines are also shown.

channels alone. We do this as one could imagine two deltas with similar total system mobility, one dominated by rapid lateral channel migration and one dominated by topographic modification through floodplain deposition with slowly moving channels. These two cases would likely produce very different stratigraphic architecture and as such determining the mode of system mobility has important implications for stratigraphic prediction, including the distributions and interconnectedness of channel fill deposits.
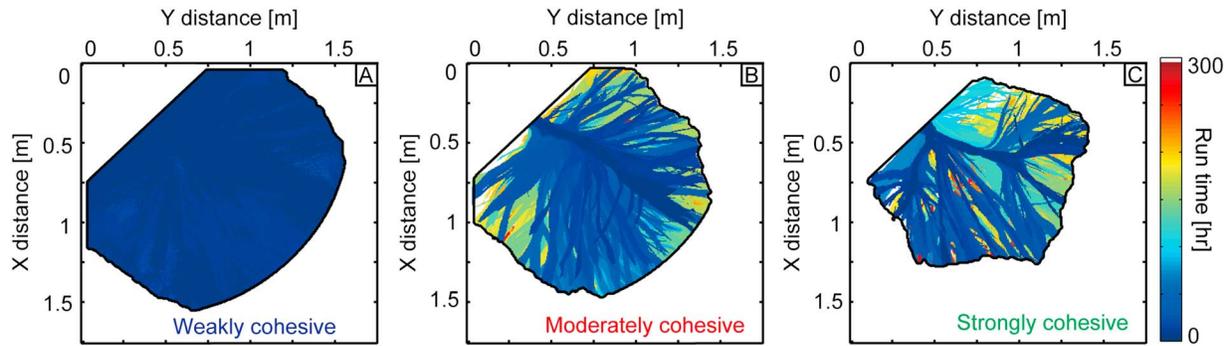
3.4.1. Terrestrial System Mobility

As we are interested in linking cohesion induced changes in the rates of key morphodynamic processes to their stratigraphic consequences, we must first measure how the magnitude of morphodynamic rates varied in our experimental stages. We start by measuring a parameter we refer to as system mobility. Previous experimental studies quantified a similar parameter by tracking the fraction of a delta top visited by flow in overhead images of the transport system (Cazanacli et al., 2002; Kim et al., 2010; Straub & Wang, 2013). In these experiments sediment was transported mainly as bed load by braided channel systems that lacked overbank flow. As such, it was safe to assume if a region was visited by flow, some geomorphic work occurred. In our experiments, particularly in the strongly cohesive stage, sediment is transported as a mixture of bed load and suspended load, and we observe significant overbanking flow, some of which lacked either the shear stresses or sediment concentrations necessary to erode or deposit sediment. Given the high temporal resolution of our topographic data, we decided to measure system mobility directly by measuring the time necessary for significant geomorphic work to occur over a wide swath of the delta-top. We refer to elevation changes, either erosion or deposition, as modifying or regrading the transport surface. We are primarily interested in modification of the terrestrial delta top, but this introduces a problem, as our terrestrial delta-top area measurements indicate that shoreline locations autogenically varied through time. As a result, some cells frequently transitioned from terrestrial to marine environments. To compensate for this, we use a constant area that corresponds to the region of each experimental surface that was land for at least 50% of the run time (Figure 4b). Here we define f_m as the fraction of delta-top area modified by a depositional or erosional event of at least 1 mm, the vertical resolution of our DEMs. As such, the unmodified fraction (f_{um}) is equal to $1 - f_m$. Using our topographic data set, we track f_{um} by monitoring the fraction of area within our $p_{land} = 50\%$ maps yet to be modified for 60 h windows, starting every 1 h of run time for each stage. The 60 h window is long enough for nearly all locations to be modified in each experiment.

The decay of f_{um} in any one stage shows tremendous variability depending on the starting hour. However, when ensemble averaging this variability, we find the following results. The average rate of f_{um} decay decreases as sediment cohesion increases, indicating that cohesion reduces lateral system mobility. Second, the variability in f_{um} decay increases as cohesion increases (Figure 5a).

Similar to Wickert et al. (2013), we fit an exponential trend to each ensemble averaged f_{um} curve (Figure 5b):

$$f_{um} = \alpha^* \exp(-\lambda_m t) \qquad (1)$$

Figure 6. (a–c) Locations modified by river channels through time. The bounding polygons in Figures 6a–6c represent the shape of the delta that was above sea level for at least 50% of each experimental stage. Locations shown in blue were visited by channelized flow rapidly after the start of each stage, while locations shown in red or white took much longer to be visited by channelized flows or were never visited by channelized flows.

where λ_m is the decay rate, a is a leading coefficient, and t is time. The estimated decay rates allow us to characterize a time scale of lateral system mobility, T_{sy}, as the time necessary for 95% of the $p_{land} = 50\%$ area to experience topographic modification. This is similar to the channel time scale definition used in previous studies (Cazanacli et al., 2002; Wickert et al., 2013) and represents an important autogenic time scale for deltas. We observe that T_{sy} increases with cohesion and is equal to 15, 30, and 40 h for the weakly, moderately, and strongly cohesive stages, respectively.

We explored use of other p_{land} values to characterize system mobility and found that while it slightly changed the absolute value of the measured parameters, it did not change the trends between experiments. For example, if we use a p_{land} value of 25%, we observe that T_{sy} still increases with an increase in cohesion and is equal to 15, 29, and 37 h for the weakly, moderately, and strongly cohesive stages, respectively.
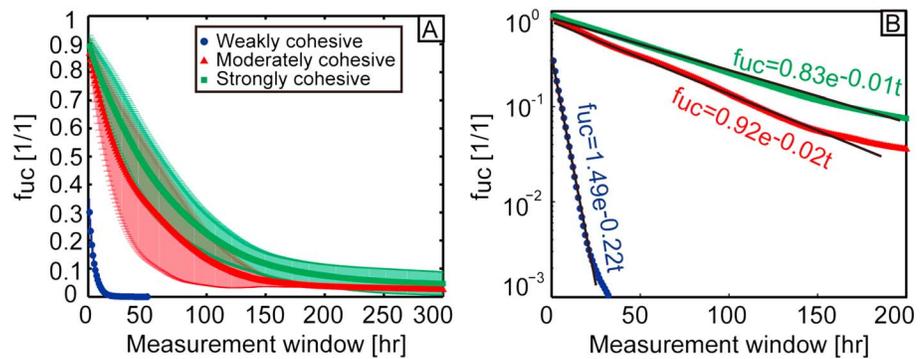
3.4.2. Terrestrial Channel Mobility

System mobility, as defined above, includes mobility that induces geomorphic modification from both channels and overbank flow. Here we isolate the influence of cohesion on just the mobility of channels. This is done to aid our ability to link changes to surface processes induced by cohesion to the partitioning of deposits in channel verses overbank environments and is accomplished with the topographic scans that were coregistered with digital images of the dyed flow field. The locations associated with active channelized flow were manually mapped for every hour of the three stages (Figure 1d). Specifically, we visually identified linear flow features that resembled channel configurations from the digital images collected by the scanner while dyed flow was turned on. The binary channel maps (1 for channel, 0 for nonchannel) were used to isolate areas modified by channelized flow.

We illustrate the spatial pattern of modification by channels by tracking the time that each delta-top pixel was first modified by channelized flow, for each experimental stage (Figure 6). We do this for the $p_{land} = 50\%$ area and over a 300 h run window for each stage. These maps suggest rapid widespread topographic modification by channels in the weakly cohesive stage and a decrease in channel mobility as cohesion increased.

We quantify the trends observed in Figure 6 by tracking the reduction in the fraction of area unmodified by channels, f_{uc}, similar to the method used for measuring f_{um}. Due to large differences in the rate of decay of f_{uc} in each stage, we use 50, 300, and 300 h windows for the weakly, moderately, and strongly cohesive stages, respectively, starting every 1 h of run time. These windows are long enough to allow channels to visit most of the $p_{land} = 50\%$ area in each stage.

Similar to the f_{um} decay curves, we observe strong variability in the decay of f_{uc}, which increases from the weakly to strongly cohesive stages (Figure 7a). To characterize a channel time scale, we fit an exponential trend to the ensemble averaged f_{uc} curves (Figure 7b). With the exponential decay rates, λ_c, we estimate the time scale of lateral channel mobility, T_{ch}, as the time necessary for 95% of the $p_{land} = 50\%$ area to experience topographic modification by channels. We observe that T_{ch} increases from the weakly to strongly cohesive experiments, which are 16, 164, and 293 h, respectively.

Figure 7. Data defining the reduction in area that has not been modified by channelized processes. (a) Data in arithmetic space, with mean decay trend represented by symbols. The vertical bars represent variability in measurements and are equal to ±1 standard deviation. (b) Decay of mean trend in semilog space to illustrate approximate exponential reduction in f_{uc}, the fraction of area unmodified by channels. Equations of best fit trends lines are also shown.

3.5. Experimental Stratigraphy

One of our overarching aims is to link differences in the statistics of the surface processes to statistics that describe stratigraphic architecture. As such, in this section, we aim to link changes in sediment cohesion to qualitative differences in the stratigraphic architecture and quantitative changes in statistics that (1) describe how space is filled in alluvial basins and (2) how sediment of different grain sizes is segregated in the stratigraphy. Given the constant forcing in each stage, differences in the resulting stratigraphy reflect differences in the spatial and temporal scales of the autogenic surface processes.

3.5.1. Synthetic and Physical Stratigraphy

We use the topographic data from each experiment to generate volumes of synthetic stratigraphy by stacking DEMs with topography clipped to account for sediment removed during erosional events (Martin et al., 2009). To compare the three experiments, we display the synthetic stratigraphy as a function of a dimensionless mass extraction parameter, χ, which represents the fraction of sediment input to a basin that has been lost to deposition upstream of a distance x (Paola & Martin, 2012; Strong et al., 2005). The volume lost to deposition is the integral of the net rate of deposition r over the area inbound of distance x. Thus, for an initial total sediment flux, Q_s, the value of χ at a given location is equal to
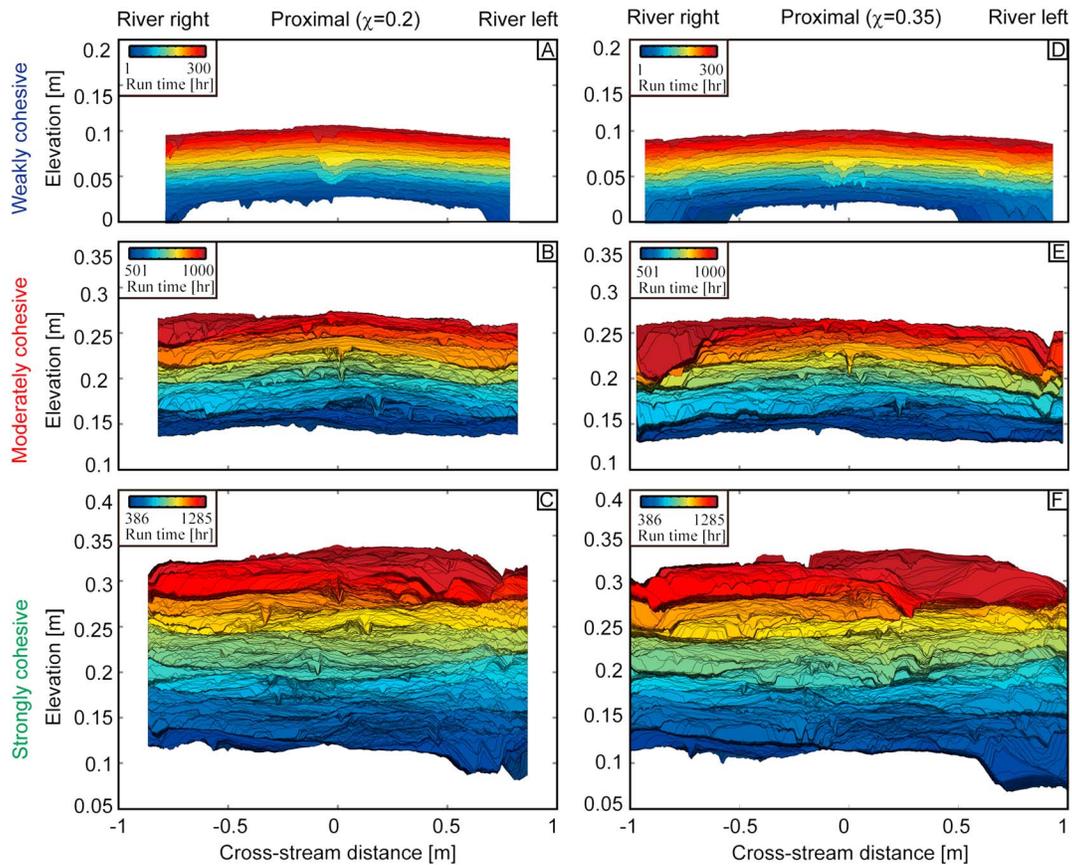
$$\chi(x) = \frac{1}{Q_S} \int_0^x B(x')r(x')dx' \qquad (2)$$

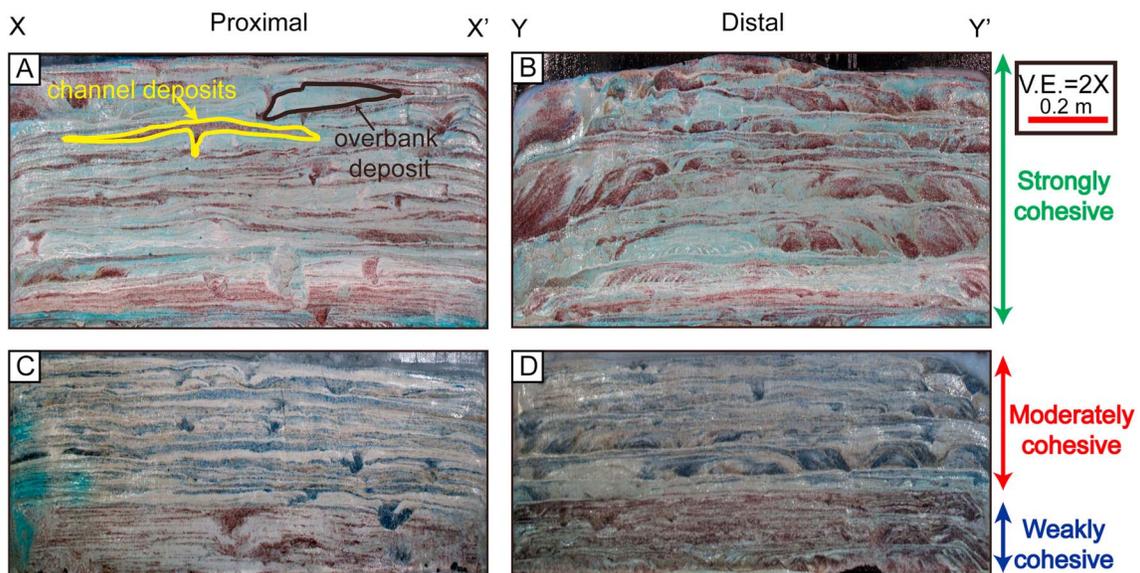 where B represents the width of a transect at a given distance of x.

In cross sections of the synthetic (Figure 8) and physical stratigraphy (Figure 9) from relatively proximal delta-top locations we observe that strongly cohesive strata (Figures 8c and 9a) are mainly composed of coarse channel fill and fine-grained overbank deposits. Prominent channel levee deposits are noted with high slopes and curvatures. Qualitatively, these levees appear to efficiently segregate the coarse channel body deposits from the fine overbank. Although the moderately cohesive strata (Figures 8b and 9c) also includes a large number of coarse channel fill deposits, the shape of the levee deposits are flatter compared with those observed in the strongly cohesive stratigraphy (Figure 9). The proximal weakly cohesive deposit (Figures 8a and 9c) is dominated by flat-lying time lines and by bed load deposits with a broad range of grain sizes intermixed. This deposit also has several large stacked coarse channel deposits in the middle of the cross sections that are the result of short-lived incisional channels. Similar trends are seen in the three distal transects (Figures 8d–8f and 9b and 9d), except that sandy channel deposits are largely replaced by sandy lobe deposits. Again, the segregation of fine from coarse sediment qualitatively appears to increase as the cohesion is increased.
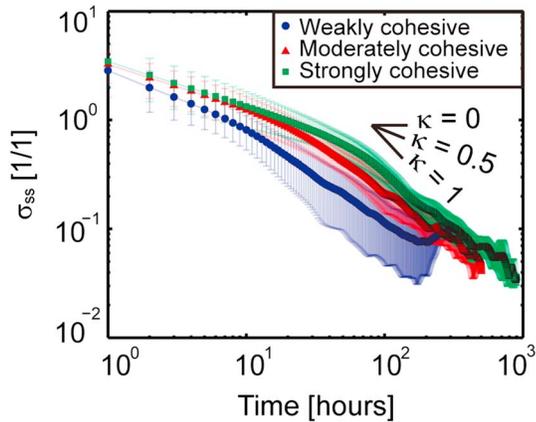
3.5.2. Compensation Metric

Overhead images and results from our statistical description of the surface dynamics indicate that sediment cohesion increases the tendency for channels to lock in place for long periods of time. We hypothesized that an increase in the cohesion within the system should increase the persistence in deposition trends in the stratigraphic record and reduce the evenness of basin fills over a range of time scales. To test these hypotheses,

Figure 8. Synthetic stratigraphy along (a–c) proximal and (d–f) distal delta-top strike oriented transects. Transects are located at equivalent mass extraction locations in each experiment corresponding to $\chi = 0.2$ and $\chi = 0.35$ for the proximal and distal transects, respectively. Location of transects for moderately cohesive case are shown in Figure 1c. Stratigraphy is colored by time of deposition in each experiment and lines represent topography clipped for erosion.

Figure 9. Photographs of preserved physical stratigraphy of the three experimental stages from a (a and c) proximal and (b and d) distal strike oriented transect. The vertical exaggeration is two times. Panels are oriented as if one was looking down system. Location of transects are shown in Figure 1b.

Figure 10. Comparison of the decay of σ_{ss}, standard deviation of the ratio of sedimentation to subsidence, as a function of time window of measurement for the three experimental stages. The vertical bars represent variability in σ_{ss} measurements and are equal to ±1 standard deviation. Higher (lower) values of σ_{ss} correspond with larger (smaller) variability in the sedimentation pattern. κ, the compensation index, ranges from 0 to 1.

we use the compensation statistic, which compares sedimentation patterns to those of the long-term generation of accommodation. Compensation describes the tendency of deposits to preferential fill topographic lows in the transport system. Straub et al. (2009) linked compensation in basin filling to the decay of the spatial variability in sedimentation between select depositional horizons as a function of increasing vertical stratigraphic averaging distance.

The variability in sedimentation patterns is quantified using the standard deviation of the ratio of sedimentation over a time window of interest to the long-term sedimentation rate (Sheets, Hickson, & Paola, 2002):

$$\sigma_{ss}(T) = \left(\int_A \left[\frac{r(T;x,y)}{\hat{r}(x,y)} - 1 \right]^2 dA \right)^{1/2} \qquad (3)$$

where r is the local sedimentation rate measured over a temporal stratigraphic interval T, x and y define horizontal coordinates, A is the area over which the calculation is performed, and $\hat{r}$ is the local long-term sedimentation (or subsidence) rate. The larger (smaller) the standard deviation of the ratio of sediment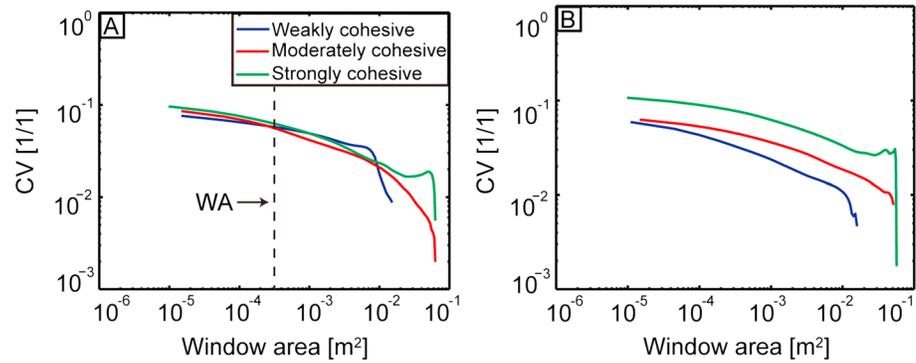ation to subsidence is, the higher (lower) the variability is in the sedimentation patterns of the system. Over long time windows, transport systems have a tendency to visit every spot in a basin repeatedly. Thus, the ratio of sedimentation to subsidence at any point in the basin should approach unity in the limit of time. However, over short time windows, depositional geometries within the basin are controlled by the configuration of the transport system. Consequently, the ratio of sedimentation to subsidence over these time scales is variable.

When calculating σ_{ss}, we use DEMs of surface topography rather than preserved stratigraphic horizons. As a result, our estimates of σ_{ss} are built from the full distribution of paleo-surface processes and include ratios of short-term sedimentation rate to long-term rates that can be both negative (erosion) and positive (deposition). Here we note that use of surface topographic data will produce slightly higher estimates of σ_{ss} than produced from stratigraphic surfaces, where only preserved deposition can be measured, but the general trends within and between experiments are the same.

Similar to Wang et al. (2011), we observe that the slope of the decay of σ_{ss} as a function of measurement time is scale-dependent (Figure 10). Previous studies showed that the exponent of this power law decay, the compensation index (κ), describes the tendency for deposits to stack compensationally, with increasing κ values associated with stronger compensation. From our plots of σ_{ss} as a function of measurement window, we make the following observations. (1) Regardless of the time window of interest, the variability in the depositional patterns, as quantified with σ_{ss}, goes up as cohesion increases. This suggests larger autogenically induced variability in stratigraphic stacking patterns of cohesive systems, which is in agreement with our qualitative observations. (2) The variability of σ_{ss} for a given time window increases as sediment cohesion increases. (3) Over short time scales the decay rate of σ_{ss}, and thus κ, is greatest for the weakly cohesive case and decreases as sediment cohesion increases. This indicates that over shorter time scales, the strength of compensation decreases as sediment cohesion increases. Over longer measurement windows this decay rate approaches 1 for all stages, which indicates complete compensation as depositional patterns match the pattern of accommodation generation. Wang et al. (2011) highlighted that the time scale associated with complete compensation, termed the compensation time (T_c), represents the upper limit of autogenic time scales in basin filling and can be estimated as the maximum scale of autogenically induced roughness on a transport system divided by the long-term, basin-wide aggradation rate. We expand on this point in the discussion section.

3.5.3. Spatial Composition Variability of Physical Stratigraphy

Understanding controls on the magnitude and spatial scales of compositional changes in stratigraphy has implications for prediction of stratigraphic properties, including the connectivity of high permeability zones. While results from our analysis of compensation indicate cohesion induced changes in the filling of accommodation, the metric used did not quantify the spatial variability of deposit composition. Here we tackle this

Figure 11. Comparison of stratigraphic spatial variability in composition as expressed by CV, the coefficient of variation, for increasing measurement window area in the three experimental stages for the (a) proximal (see transect XX′ in Figure 1b) and (b) distal (see transect YY′ in Figure 1b) physical stratigraphic panels.

question using a metric which quantifies segregation of fine and coarse particles over a range of spatial scales. To accomplish this, we use spatial changes in the intensity of color in the physical stratigraphic sections as a proxy for the spatial composition variability. We use the three color bands, R, G, and B, captured by digital images of the stratigraphy to calculate the red intensity in each pixel of the deposits:

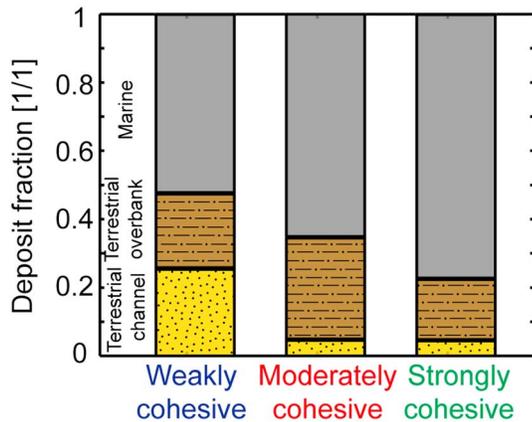$$I = \frac{R - G - B + 2^*C_{max}}{3^*C_{max}} \tag{4}$$

where C_{max} is the maximum possible value for each color band and here is equal to 255.

To quantify sediment segregation by particle size, we quantify the coefficient of variation, CV, of the sediment color intensity in square measurement windows over the extent of each stratigraphic panel. For a given measurement window, CV is calculated as
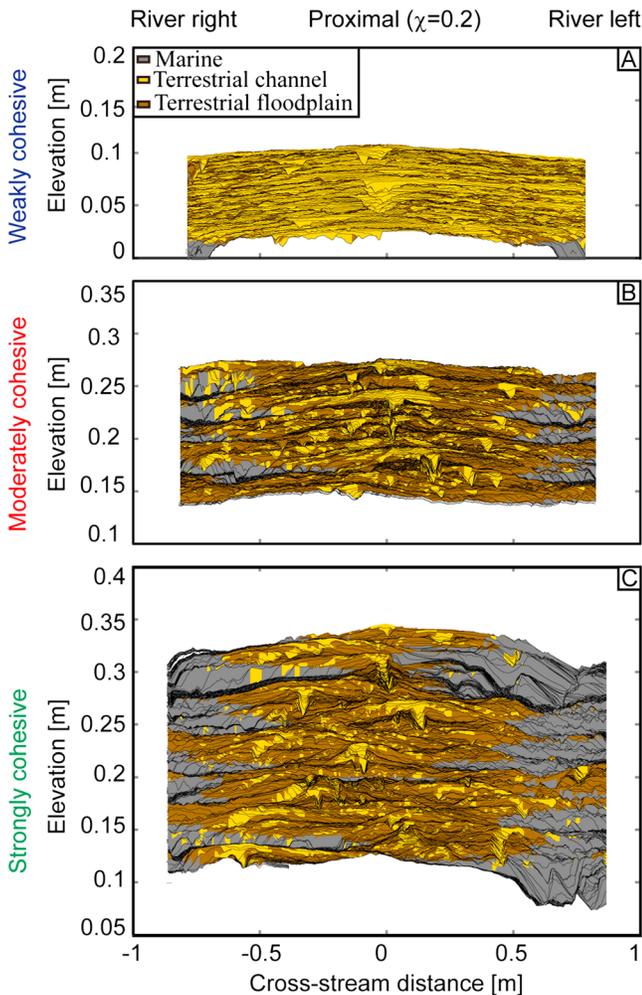
$$CV = \frac{\sqrt{\frac{1}{N}\sum_{i=1}^{N}\left(I_i - \bar{I}\right)^2}}{\bar{I}} \tag{5}$$

where N is the total number of square measurement windows of a specified size within the stratigraphic panel of interest, $\bar{I}$ is the mean normalized color intensity, and I_i is the normalized color intensity in each square measurement window of the panel. We then track how CV varies as a function of the size of a measurement window (Figure 11). We do this calculation for windows with sizes ranging from 10 by 10 image pixels (~1.5×10^{-5} m^2) to ~0.015 m^2.

Qualitatively, we noted that an increase in cohesion resulted in the separation of fine (white) from coarse (either red or blue) sediment. As cohesion increased, the fines were largely sequestered in overbank deposits while the coarse material dominantly was stored in channel fill and lobe deposits (Figure 9). Quantitatively, if strong segregation of fine and coarse material is present, there will be locations with high color intensity (sandy material) and locations with low color intensity (fine material). As a result, the CV of these intensities would be high. If segregation is minimal, most windows, at the measurement size of interest, will have roughly the same intensity and CV will be low. Over small measurement windows, we observe that CV of the stratigraphy increases as the cohesion of the sediment increases for both the proximal and distal sections (Figure 11). The ordering of CV between stages for the proximal section is dependent on the window size. At a window size approximately equal to 240 mm^2 the CV of the three experiments converges and at larger window sizes the ordering of stages is reversed relative to what is observed at small window sizes. We note that this window size is approximately the scale of the channel sand bodies in the three experiments, suggesting that the qualitative segregation we observe largely happens at scales finer than a channel sand body. We also note that if the same ratio of fine to coarse material exists in two sections, they should have equal CV measurements at window sizes that are, at a minimum, the size of the deposit.

Figure 12. Percent of stratigraphic volume deposited in terrestrial channel, terrestrial overbank, and marine environments in the three experimental stages.

Figure 13. Synthetic stratigraphy along the proximal delta-top strike oriented transects. Transects are located at equivalent mass extraction locations in each experiment corresponding to χ = 0.2. Location of transect for moderately cohesive case is shown in Figure 1c. Stratigraphy is colored by environment of deposition and lines represent topography clipped for erosion.

3.5.4. Preserved Sediment Volume by Depositional Environment

Stratigraphic analyses in this study show that an increase in sediment cohesion increases sediment segregation and depositional persistence (the tendency to deposit in one location for a long period of time). However, we are unclear if this increase in depositional persistence is correlated with changes in the volume of sediment preserved in stratigraphy from various depositional environments. To determine this, we use the channel maps and synthetic stratigraphy to measure the fraction of the stratigraphy deposited in terrestrial channels, terrestrial overbank, and marine environments, relative to the total volume of sediment input to the basin. We first use the synthetic stratigraphy to calculate sediment volumes preserved between two consecutive scans. Next, using the maps of channel locations and the imposed sea level, we separate this volume into our three depositional environments. Unfortunately, deep ocean water depths (>50 mm or approximately >4 channel depths), in later parts of the experiments, prevented us from measuring topography for most of the marine environment. We did observe a large volume of prodelta sediment when draining and cleaning the basin after each experiment. Given our nearly universal coverage of terrestrial settings, we assume that any sediment input to the basin that is not accounted for in our synthetic stratigraphy was deposited in a marine environment.

With our final inventory of sediment volumes from each depositional environment, we make the following observations. As sediment cohesion increased, the fraction of sediment deposited in the terrestrial (channel and overbank) environment decreased from the weakly to strongly cohesive stages (Figures 12 and 13). This is consistent with the results of Straub et al. (2015), who found that an increase in sediment cohesion decreased deltaic retention rates.

Second, the fraction of channel deposits decreased from the weakly to strongly cohesive stages (Figure 12). Finally, we note that the volume of terrestrial overbank deposits increased from the weakly cohesive to moderately cohesive stage but then decreased for the strongly cohesive stage. We hypothesize that this trend is related to the change in delta size between stages. It is possible that overbanking flow increased progressively as sediment cohesion increased. However, the small delta area in the strongly cohesive case allowed some sediment transported out of channels to be advected to the marine environment, where it was deposited.

4. Discussion

4.1. Influence of Sediment Cohesion on Surface Dynamics: System and Channel Mobility Numbers

In this study, we systematically quantify how an increase in sediment cohesion influences the spatial and temporal scales of deltaic autogenic processes. Our GEMS experiments could not differentiate the erodibility of the moderately and strongly cohesive sediment mixtures. This is possibly due to the fact that the maximum shear stress that the GEMS system can apply is less than the critical shear stress of the moderately and strongly cohesive sediment mixture. In addition, the reason why the eroded mass in the moderately cohesive experiment, below 0.2 Pa, is larger than that in weakly cohesive experimental stage

might be related to a visually undetectable perturbation of upper layer of the sediment cores. However, our statistical characterization shows clear differences between the three stages. One of the major findings in the surface dynamics is that an increase of sediment cohesion reduces both system and channel lateral mobility and thus increases the autogenic time scales necessary to regrade the deltaic topography, through channels or a combination of both channelized and overbank flow. This observation is consistent with previous studies, which note that sediment cohesion promotes channelization and decreases channel lateral mobility (Caldwell & Edmonds, 2014; Edmonds & Slingerland, 2010; Martin et al., 2009; Straub et al., 2015).

An increase in sediment cohesion also changes the configuration of the transport system in our experiments from sheet-flow to channelized-flow. This change in fluvial style, induced by sediment cohesion, could play an important role in the evolution of river delta surfaces. In our weakly cohesive experiment, channelized flows do not stay in place for a long time. This results in a smoother deltaic surface. In contrast, the deltaic surfaces in the moderately and strongly cohesive experimental stages are rougher due to an increase in depositional persistence induced by sediment cohesion. These results are supported by the synthetic stratigraphy (Figure 8). For field-scale systems, one might compare the Yellow and Mississippi River Delta systems. As Edmonds and Slingerland (2010) note, these two systems share similar boundary and forcing conditions; however, the sediment of the Mississippi River system is far more cohesive than the Yellow River system. Our results suggest that deltaic surfaces and associated stratigraphic surfaces might be smother in less cohesive systems, such as Yellow River Delta, compared with more cohesive systems such as the Mississippi River Delta or also the Ganges Delta, which has dense vegetation.

To further explore how sediment cohesion influences system and channel mobility and link these dynamics to possible stratigraphic architecture, we define two dimensionless numbers that compare lateral mobility to vertical mobility over basin-filling time scales. Specifically, we define a basin-filling system mobility number, M_s, and a basin-filling channel mobility number, M_c as
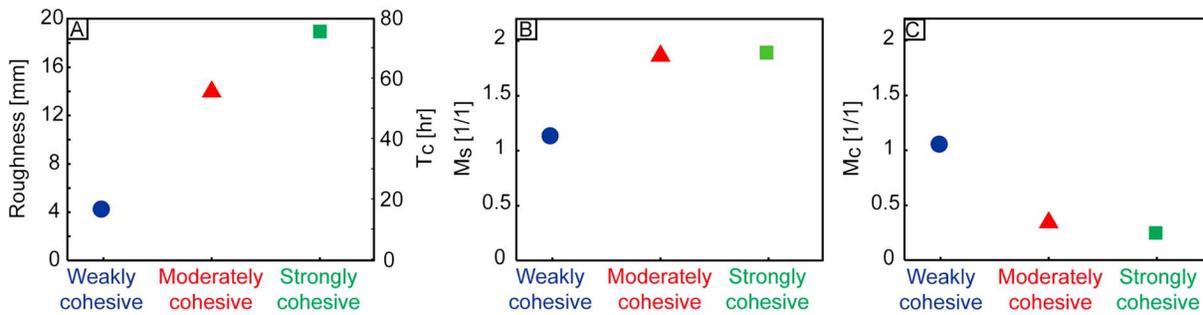
$$M_s = \frac{h/v}{T_{sy}} = \frac{T_c}{T_{sy}} \tag{6}$$

$$M_C = \frac{h/v}{T_{ch}} = \frac{T_c}{T_{ch}} \tag{7}$$

where h is the maximum autogenic roughness length of the transport system, v is the basin-wide long-term aggradation rate, and T_c is the compensation time scale or the time necessary to aggrade, on average, one vertical roughness scale everywhere in the basin (Wang et al., 2011). The spirit behind M_c and M_s is similar to a short-time scale mobility number proposed by Jerolmack and Mohrig (2007), who compare the time necessary for a single channel to aggrade one channel depth to the time necessary to laterally migrate one channel width.

We are interested in relating M_s and M_c to characteristics of the stratigraphic architecture (Figure 14). We note that M_s, by itself, might not be particularly useful in predicting stratigraphic architecture. We can imagine two systems with equally high mobility, one coming from rapidly migrating channel bodies with limited overbank deposition and a second system defined by slow moving channels, but frequent overbanking flow that is able to modify floodplains. Similar to the short-time scale mobility number of Jerolmack and Mohrig (2007), we propose that the relative magnitude of M_c is related to the propensity of channel deposits to contain evidence for vertical versus lateral migration. As such, systems defined by high M_c should have channel deposits with widths much greater than the channels that deposited them, while channel bodies of low M_c systems will have channel body widths of similar magnitude to their paleo-channel forms.

To estimate either of our mobility numbers, we first must measure h. To do this, we detrend each topographic map for the long-term basin-wide deposition rate imposed by the base level rise. Next, we detrend each map for the long-term average spatial structure of topography. This second step is necessary as the migration of channels over the delta top, originating at the basin infeed location at the center of the proximal wall, resulted in an average symmetric convex-up profile of topography for all strike-oriented transects, with on average the highest topography located in the center of the basin. In addition, to drive transport of sediment toward the ocean, an average down-stream slope was present that must be accounted for prior to estimating h. We define h as the difference of the 97.5 and 2.5 percentiles of the detrended elevation distribution. We

Figure 14. Measurements of (a) deltaic roughness and associated calculation of compensation time which are used to measure the system. T_c is the compensation time scale, the time to deposit one channel-depth worth of stratigraphy everywhere in the (b) delta basin and (c) channel mobility numbers over basin-filling time scales for the three experimental stages. M_s and M_c are system and channel mobility number, respectively.

find that this roughness length scale, and thus the compensation time scale, increases as sediment cohesion increases (Figure 14a). T_c has been defined as the maximum autogenic time scale in basin-filling (Wang et al., 2011). As such, our results indicate that increasing sediment cohesion increases both the temporal scales of autogenic lateral mobility and autogenic space filling. Thus, our basin-filling mobility numbers allow us to examine if lateral mobility decreases faster than vertical space filling mobility as cohesion is increased.

The estimates for T_c allow us to calculate M_s and M_c for each stage (Figures 14b and 14c). We find that increasing sediment cohesion actually increases M_s in our experiments, suggesting that addition of cohesion causes the vertical space filling mobility to decrease faster than the decrease observed in lateral system mobility. Put another way, the trend in M_s indicates that increasing sediment cohesion resulted in a stronger response to the growth of surface roughness (i.e., channel deepening) than the commensurate decrease in lateral mobility.

As expected, the increase in cohesion is associated with a significant decrease in the channel mobility numbers over basin-filling time scales (Figure 14). Combined, the trends in M_s and M_c suggest that while increasing sediment cohesion slows the movement of channels, it also results in deeper channels with faster moving flow that can transport suspended sediment to overbank environments where it can modify topography. We also see that M_c for the moderately and strong cohesive stages is significantly less than 1, meaning that over the course of $1 - T_c$ channels generally do not visit all basin locations. Coupling this with the significant system mobility attributed to overbank activity should result in stratigraphy dominated by isolated channel bodies with widths that are similar to their geomorphic forms and isolated channels that are encased in overbank deposits. These predictions match observations of the architecture in our physical stratigraphic panels.

4.2. Linking Deltaic Surface Dynamics With Subsurface Stratigraphy

Straub et al. (2015) used the same set of experiments discussed here to show how sediment cohesion increases scales of autogenic shoreline transgressions and regressions and how this could influence the scales of autogenic parasequences. In this study, we are focused on the changes in deltaic morphodynamics and specifically the stratigraphic characteristics associated with varying levels of sediment cohesion. A summary of our results indicates that increasing cohesion is linked to the following stratigraphic consequences: (1) increased variability of depositional patterns relative to the generation of accommodation, (2) increased segregation of fine from coarse sediment, and (3) a decrease in the volume of sediment deposited in terrestrial channel environments and a decrease in sediment deposited in terrestrial settings because of the relative increase in the percentage of sediment deposition in the marine environment.

We link the enhanced variability in depositional patterns to the strong depositional persistence induced by the reduction in the lateral mobility of the total system, and significantly the channels, due to cohesion. This reduction in lateral mobility can also be linked to our other stratigraphic observations. Long periods with relatively stable channel configurations allowed thick overbank deposits to accumulate from the overspill of suspended sediment-laden flow from channels. Sediment suspended in this overspill was fine-grained, while in-channel deposition was dominated by the coarse sediment moved primarily as bed load. Combined, these factors led to the segregation of the fine from coarse sediment as sediment cohesion increased. This could

suggest that paleo-systems imaged in outcrops with well-documented clean and coarse channel sands encased in fine grained deposits (e.g., Brushy Basin Member of the Morrison Formation, Utah, USA (Heller et al., 2015)) were more cohesive than systems that produced outcrops which lack strong segregation by particle size (e.g., Castlegate Sandstone (Hajek & Heller, 2012)). Finally, in our experiments the reduction in channel mobility allowed channels to act as continuous conveyor belts of large sediment volumes to the marine environment for long periods before eventual channel avulsion and reorganization. This reduced terrestrial sediment trapping and led to the observed changes in the relative volumes of sediment deposited in the three depositional environments-terrestrial channel, terrestrial overbank, and deep marine.

In our experiments the material transported to the marine environment was dominantly the fine-grained component of the input particle size distribution. Thus, our result of increased marine deposition as cohesion increased suggests that strongly cohesive field-scale systems (e.g., the Mississippi River Delta) will generate terrestrial stratigraphy that is on average coarser grained than similar weakly cohesive systems (e.g., the Yellow River Delta). Due to segregation of particles by size in the strongly cohesive terrestrial deposits, this should produce channel deposits enriched in coarse particles, but also volumetrically significant overbank strata that are near devoid of coarse material. It is only when averaging these two facies types together that the strongly cohesive terrestrial strata are coarser than similar weakly cohesive systems.

Our results might also aid interpretation of changes in the stratigraphic record from the Cambrian to Devonian. As noted by Davies and Gibling (2010), the percentage of stratigraphic sections with significant mudrock increased after the rise of vascular plants, starting in the early Silurian, ~436 Ma, as did the presence of single thread meandering rivers. Quantification of this trend by Davies and Gibling, made with a database of stratigraphic facies as a function of age of deposition, supported long standing theory that the rise of vegetation influenced the nature of the physical stratigraphic record (Cotter, 1977; Fuller, 1985; Long, 2004; Macnaughton, Dalrymple, & Narbonne, 1997; Schumm, 1968) Davies and Gibling (2010) provide the following mechanisms to explain the increase in mudrock preservation after the rise of vascular vegetation: (a) a reduction in aeolian winnowing of floodplain fines as a result of increased boundary friction from vegetation stalks which can reduce flow speed and thus transport capacity, (b) an increase in the retention of fines in the alluvial system by increasing tensional strength in fine-grained sediment through rooting, (c) an increase in the production of clays through chemical weathering associated with bio-geo-chemical activity, and (d) an increase in perennial fluvial flow by increasing evapotranspiration and precipitation. We would add the following mechanism: The increase in sediment cohesion provided by rooting promotes deep stable channels, which can shed significant volumes of fines to floodplains during bankfull flow events. These thick floodplain deposits are then difficult to completely remove or rework during system reorganization (avulsion) events.

4.3. Implications for Environmental Signal Storage in Stratigraphy

In addition to the ratio of sediment to water discharge entering a deltaic environment (Straub & Wang, 2013), basin water depth (Carlson, Kim, & Piliouras, 2013), and tectonic setting (Kim et al., 2010; Straub et al., 2013), our results highlight the importance of sediment cohesion in setting the spatial and temporal scales of autogenic processes. Specifically, we find that sediment cohesion increases the maximum depth of a system's channels, which is often considered to be an important vertical autogenic length scale. Sediment cohesion also influences two important autogenic time scales. First, as the compensation time scale is linked to the amount of time necessary to aggrade one channel depth, it follows that an increase in channel depth will increase T_c, all else being equal. Second, the reduction in channel mobility increases the amount of time necessary for channels to visit all locations on a delta and thus do geomorphic work.

Previous studies (Jerolmack & Paola, 2010; Li, Yu, & Straub, 2016) highlighted that the autogenic length and time scales mentioned above help set thresholds for the storage of environmental signals in stratigraphy. For example, (Li et al., 2016) note that the extraction of relative sea Level (RSL) cycle signals from the physical stratigraphic record requires their magnitudes and periodicities to be greater than the spatial and temporal scales of the autogenic dynamics of deltas. Coupling our results with the findings of Li et al. (2016) suggest that coarse-grained and/or low vegetation density deltas might be more sensitive to changing environmental conditions, compared to fine-grained and/or densely vegetated deltas. As such, coarse-grained and/or low vegetation density deltas might better store information in stratigraphy pertaining to changing environmental conditions.

Interestingly, both the Mississippi and Ganges deltaic depocenters are covered by dense vegetation and were highlighted by Li et al. (2016) as having autogenic length and time scales that might prevent extraction of high-frequency and low-magnitude RSL cycles from their stratigraphy. We suggest that the dense vegetation in these systems enhances autogenic channel depths in comparison to less cohesive systems like the Yellow River Delta (Edmonds & Slingerland, 2010). This leads us to suggest that the optimal conditions for storing environmental signals include systems with shallow channels, resulting from either low sediment cohesion and/or low ratios of water to sediment flux, and basins with high long-term subsidence rates.

5. Summary

Using physical experiments, we examine the influence of sediment cohesion on the spatial and temporal scales of deltaic surface dynamics and how these surface processes set stratigraphic architecture over basin-filling time scales. Building on previous studies, we use metrics to quantify how the addition of cohesion influences key autogenic process and product scales. The main results are summarized as follows:

1. Sediment cohesion promotes the development of deep, laterally stable channels. The low lateral mobility of cohesive systems reduces the capacity to laterally distribute sediment. As a result, the temporal and spatial scales of autogenic shoreline transgressions increase with cohesion. This reduces the area of deltas that is consistently above sea level.
2. Using topographic data and maps of channel locations, we calculate an autogenic time scale for topographic modification and a time scale for modification by channels in each experimental stage. The first time scale is set by the lateral mobility of the total transport system (overbank + channels), while the second is set just by the lateral mobility of channels. Sediment cohesion is linked to a reduction in lateral mobility of both the total transport system and the channels. However, the reduction in lateral channel mobility is greater than that of the total system, indicating that sediment cohesion aids the transport of sediment-laden flow to overbank settings, where it can modify topography and fill space.
3. Depositional timelines indicate that cohesion enhances depositional persistence. This enhanced persistence reduces the match between patterns of deposition and patterns of accommodation generation over a wide range of time scales. This suggests a link between autogenic time scales that quantify surface mobility and the autogenic scales present in stratigraphy.
4. Observations of the experimental physical stratigraphy suggest that cohesion increases the segregation of coarse material into channels and lobes while the fine material is segregated into overbank deposits. This segregation is linked to a decrease in the total volume of channel relative to overbank deposits in the preserved record.

References

Beerbower, J. R. (1964). Cyclothems and cyclic depositional mechanisms in alluvial plain sedimentation. Paper presented at Symposium on Cyclic Sedimentation: State Geological Survey of Kansas, Bulletin.

Braudrick, C. A., Dietrich, W. E., Leverich, G. T., & Sklar, L. S. (2009). Experimental evidence for the conditions necessary to sustain meandering in coarse-bedded rivers. *Proceedings of the National Academy of Sciences of the United States of America*, *106*(40), 16,936–16,941.

Burpee, A. P., Slingerland, R. L., Edmonds, D. A., Parsons, D., Best, J., Cederberg, J., … Royce, J. (2015). Grain-size controls on the morphology and internal geometry of river-dominated deltas. *Journal of Sedimentary Research*, *85*(6), 699–714.

Caldwell, R. L., & Edmonds, D. A. (2014). The effects of sediment properties on deltaic processes and morphologies: A numerical modeling study. *Journal of Geophysical Research: Earth Surface*, *119*, 961–982. https://doi.org/10.1002/2013JF002965

Carlson, B., W. Kim, & A. Piliouras (2013). Basin depth control on the autogenic timescale of fluviodeltaic systems. Paper presented at AGU Fall Meeting Abstracts.

Cazanacli, D., Paola, C., & Parker, G. (2002). Experimental steep, braided flow: Application to flooding risk on fans. *Journal of Hydraulic Engineering*, *128*(3), 322–330.

Cotter, E. (1977). The evolution of fluvial style, with special reference to the central Appalachian Paleozoic. In A. D. Miall (Ed.), *Fluvial sedimentology* (Vol. 5, pp. 361–384). Calgary: Canadian Society of Petroleum Geologists Memoir.

Davies, N. S., & Gibling, M. R. (2010). Cambrian to Devonian evolution of alluvial systems: The sedimentological impact of the earliest land plants. *Earth-Science Reviews*, *98*(3), 171–200.

Davies, N. S., & Gibling, M. R. (2011). Evolution of fixed-channel alluvial plains in response to Carboniferous vegetation. *Nature Geoscience*, *4*(9), 629–633.

Edmonds, D. A., & Slingerland, R. L. (2010). Significant effect of sediment cohesion on delta morphology. *Nature Geoscience*, *3*(2), 105–109.

Fuller, A. (1985). A contribution to the conceptual modelling of pre-Devonian fluvial systems. *South African Journal of Geology*, *88*(1), 189–194.

Galloway, W. E. (1975). Process framework for describing the morphologic and stratigraphic evolution of deltaic depositional systems. In M. L. Broussard (Ed.), *Deltas: Models for exploration* (pp. 87–98). Houston, TX: Houston Geological Society.

Gibling, M. R. (2006). Width and thickness of fluvial channel bodies and valley fills in the geological record: A literature compilation and classification. *Journal of Sedimentary Research*, *76*(5), 731–770.

Grabowski, R. C., Droppo, I. G., & Wharton, G. (2011). Erodibility of cohesive sediment: The importance of sediment properties. *Earth-Science Reviews*, *105*(3), 101–120.

Gust, G., & Müller, V. (1997). Interfacial hydrodynamics and entrainment functions of currently used erosion devices. In N. Burt, R. Parker, & J. Watts (Eds.), *Cohesive sediments* (pp. 149–174). Chichester: Wiley.

Hajek, E., & Heller, P. (2012). Flow-depth scaling in alluvial architecture and nonmarine sequence stratigraphy: Example from the Castlegate Sandstone, central Utah, USA. *Journal of Sedimentary Research*, *82*(2), 121–130.

Heller, P. L., Ratigan, D., Trampush, S., Noda, A., McElroy, B., Drever, J., & Huzurbazar, S. (2015). Origins of bimodal stratigraphy in fluvial deposits: An example from the Morrison Formation (Upper Jurassic), Western USA. *Journal of Sedimentary Research*, *85*(12), 1466–1477.

Hicks, D. M., Duncan, M. J., Walsh, J. M., Westaway, R. M., & Lane, S. N. (2002). New views of the morphodynamics of large braided rivers from high-resolution topographic surveys and time-lapse video. In F. J. Dyer, M. C. Thomas, & J. M. Olley (Eds.), *The structure, function and management implications of fluvial sedimentary systems* (pp. 373–380). Wallingford: IAHS Publication.

Hooke, R. L. (1968). Model geology: Prototype and laboratory streams: Discussion. *Geological Society of America Bulletin*, *79*(3), 391–394.

Hoyal, D., & Sheets, B. (2009). Morphodynamic evolution of experimental cohesive deltas. *Journal of Geophysical Research*, *114*, F02009. https://doi.org/10.1029/2007JF000882

Jerolmack, D. J., & Mohrig, D. (2007). Conditions for branching in depositional rivers. *Geology*, *35*(5), 463–466.

Jerolmack, D. J., & Paola, C. (2010). Shredding of environmental signals by sediment transport. *Geophysical Research Letters*, *37*, L19401. https://doi.org/10.1029/2010GL044638

Kim, W., & Jerolmack, D. J. (2008). The pulse of calm fan deltas. *The Journal of Geology*, *116*(4), 315–330.

Kim, W., Sheets, B. A., & Paola, C. (2010). Steering of experimental channels by lateral basin tilting. *Basin Research*, *22*(3), 286–301.

Kleinhans, M. G., van Dijk, W. M., van de Lageweg, W. I., Hoyal, D. C., Markies, H., van Maarseveen, M., … Hoendervoogt, R. (2014). Quantifiable effectiveness of experimental scaling of river-and delta morphodynamics and stratigraphy. *Earth-Science Reviews*, *133*, 43–61.

Kolb, C. R. (1963). Sediments forming the bed and banks of the lower Mississippi River and their effect on river migration. *Sedimentology*, *2*(3), 227–234.

Li, Q., & Straub, K. M. (2017a). TDB_12_1, SEAD. https://doi.org/10.5967/M03N21GX

Li, Q., & Straub, K. M. (2017b). TDB_13_1, SEAD. https://doi.org/10.5967/M07D2S7Q

Li, Q., Yu, L., & Straub, K. M. (2016). Storage thresholds for relative sea-level signals in the stratigraphic record. *Geology*, *44*(3), 179–182.

Long, D. (2004). Precambrian rivers. In *The Precambrian Earth: Tempos and events* (pp. 660–663). Amsterdam: Elsevier.

Macnaughton, R. B., Dalrymple, R. W., & Narbonne, G. M. (1997). Early Cambrian braid-delta deposits, MacKenzie Mountains, north-western Canada. *Sedimentology*, *44*(4), 587–609.

Martin, J., Sheets, B., Paola, C., & Hoyal, D. (2009). Influence of steady base-level rise on channel mobility, shoreline migration, and scaling properties of a cohesive experimental delta. *Journal of Geophysical Research*, *114*, F03017. https://doi.org/10.1029/2008JF001142

Murray, A. B., & Paola, C. (2003). Modelling the effect of vegetation on channel pattern in bedload rivers. *Earth Surface Processes and Landforms*, *28*(2), 131–143.

Nardin, W., & Edmonds, D. A. (2014). Optimum vegetation height and density for inorganic sedimentation in deltaic marshes. *Nature Geoscience*, *7*(10), 722–726.

Orton, G., & Reading, H. (1993). Variability of deltaic processes in terms of sediment supply, with particular emphasis on grain size. *Sedimentology*, *40*(3), 475–512.

Paola, C. (2016). *A mind of their own: Recent advances in autogenic dynamics in rivers and deltas* (Vol. 106, pp. 5–17). Grand Junction, CO: SEPM Special Volume.

Paola, C., & Martin, J. M. (2012). Mass-balance effects in depositional systems. *Journal of Sedimentary Research*, *82*(6), 435–450.

Peakall, J., Ashworth, P. J., & Best, J. L. (2007). Meander-bend evolution, alluvial architecture, and the role of cohesion in sinuous river channels: A flume study. *Journal of Sedimentary Research*, *77*(3), 197–212.

Rosen, T., & Xu, Y. J. (2013). Recent decadal growth of the Atchafalaya River Delta complex: Effects of variable riverine sediment input and vegetation succession. *Geomorphology*, *194*, 108–120.

Schumm, S. (1968). Speculations concerning paleohydrologic controls of terrestrial sedimentation. *Geological Society of America Bulletin*, *79*(11), 1573–1588.

Sheets, B., Hickson, T., & Paola, C. (2002). Assembling the stratigraphic record: Depositional patterns and time-scales in an experimental alluvial basin. *Basin Research*, *14*(3), 287–301.

Straub, K. M., Li, Q., & Benson, W. M. (2015). Influence of sediment cohesion on deltaic shoreline dynamics and bulk sediment retention: A laboratory study. *Geophysical Research Letters*, *42*, 9808–9815. https://doi.org/10.1002/2015GL066131

Straub, K. M., Paola, C., Kim, W., & Sheets, B. (2013). Experimental investigation of sediment-dominated vs. tectonics-dominated sediment transport systems in subsiding basins. *Journal of Sedimentary Research*, *83*(12), 1162–1180.

Straub, K. M., Paola, C., Mohrig, D., Wolinsky, M. A., & George, T. (2009). Compensational stacking of channelized sedimentary deposits. *Journal of Sedimentary Research*, *79*(9), 673–688.

Straub, K. M., & Wang, Y. (2013). Influence of water and sediment supply on the long-term evolution of alluvial fans and deltas: Statistical characterization of basin-filling sedimentation patterns. *Journal of Geophysical Research: Earth Surface*, *118*, 1602–1616. https://doi.org/10.1002/jgrf.20095

Strong, N., Sheets, B., Hickson, T., & Paola, C. (2005). A mass-balance framework for quantifying downstream changes in fluvial architecture. *Fluvial Sedimentology VII, Special Publication, International Association of Sedimentologists*, *35*, 243–253.

Tal, M., & Paola, C. (2007). Dynamic single-thread channels maintained by the interaction of flow and vegetation. *Geology*, *35*(4), 347–350.

Tal, M., & Paola, C. (2010). Effects of vegetation on channel morphodynamics: Results and insights from laboratory experiments. *Earth Surface Processes and Landforms*, *35*(9), 1014–1028.

Tornqvist, T. E. (1993). Holocene alternation of meandering and anastomosing fluvial systems in the Rhine-Meuse delta (central Netherlands) controlled by sea-level rise and subsoil erodibility. *Journal of Sedimentary Research*, *63*(4), 683–693.

Wang, Y., Straub, K. M., & Hajek, E. A. (2011). Scale-dependent compensational stacking: An estimate of autogenic time scales in channelized sedimentary deposits. *Geology*, *39*(9), 811–814.

Wickert, A. D., Martin, J. M., Tal, M., Kim, W., Sheets, B., & Paola, C. (2013). River channel lateral mobility: Metrics, time scales, and controls. *Journal of Geophysical Research: Earth Surface*, *118*, 396–412. https://doi.org/10.1029/2012JF002386

Xu, K., Bentley, S. J., Robichaux, P., Sha, X., & Yang, H. (2016). Implications of Texture and Erodibility for Sediment Retention in Receiving Basins of Coastal Louisiana Diversions. *Water*, *8*(1), 26.